



Synthesis and characterization of nanoparticles of cobalt and nickel ferrites for elimination of hazardous organic dyes from industrial wastewater

Dharmaraj J. Patil¹ · Sailesh N. Behera^{1,2}

Received: 25 August 2022 / Accepted: 17 February 2023 / Published online: 1 March 2023
© The Author(s), under exclusive licence to Springer-Verlag GmbH Germany, part of Springer Nature 2023

Abstract

This study presents the results of synthesis and characterization of nanoparticles of cobalt ferrite (CoFe_2O_4) and nickel ferrite (NiFe_2O_4) using co-precipitation method followed by application for removal of hazardous organic textile dyes of thiazole yellow G (TYG) and alizarin yellow R (AYR). XRD analysis confirmed formation of cubic spinel structure with average crystallite sizes at 16.07 nm and 13.84 nm for CoFe_2O_4 and NiFe_2O_4 , respectively. Field emission scanning electron microscopy (FESEM) analysis showed agglomeration of spherical shape morphology with uniformly distributed Co, Ni, Fe, and O elements. The surface area calculated from Brunauer–Emmett–Teller (BET) analysis was 64 m^2/g and 62 m^2/g for CoFe_2O_4 and NiFe_2O_4 , respectively. Vibrating sample magnetometer (VSM) showed super-paramagnetic behavior for all samples with magnetic saturation (M_s) at 7.269 and 6.61 emu/g for CoFe_2O_4 and NiFe_2O_4 , respectively. The adsorption influencing parameters such as pH of solution, quantity of adsorbent, and contact time on dye removal efficiency were thoroughly investigated. Overall, acidic condition of samples with pH at 4 favored the maximum removal efficiency by CoFe_2O_4 as 98, 97, and 93%, and by NiFe_2O_4 as 96, 93, and 92%, respectively, for TYG, AYR, and mixture sample. The Langmuir adsorption isotherm model describes the equilibrium of all samples with the best fit of coefficient of determination (R^2). The adsorption results fitted well with a pseudo-second-order kinetic model for all samples. The regeneration-reuse ability of adsorbents and cost estimation analysis of the dye removal process suggested that the economic suitability of nano-adsorbents for remediation of textile effluents was favored. The estimated thermodynamic parameters inferred that the removal of organic dyes onto the surface of CoFe_2O_4 and NiFe_2O_4 is a spontaneous, favorable, and exothermic physical adsorption process.

Keywords Magnetic nano-adsorbent · Co-precipitation method · Adsorption isotherms-kinetics-thermodynamics · Hazardous organic textile dyes · Regeneration-reuse capacity

Introduction

Upgradations of unit processes with modernized operational methods in various sectors of industries, agriculture, and urban set-ups across the world have caused generation of

large quantities of contaminants including organics, inorganics, and synthetic dyes (Asgharnejad et al. 2021; Kamyab et al. 2022). The fate of these contaminants depends on physical, chemical, and biological characteristics of effluents discharged into water bodies. In this context, the discharge of industrial wastewater into water bodies has drawn special attention of responsible stakeholders due to its unique characteristics of having higher loadings of toxic or hazardous components such as organics, trace elements, synthetic dyes, and many others (Ajiboye et al. 2021; Wang et al. 2022). Hence, fast development in industrialization with various multi-functional manufacturing processes has been a concern for the scientific community to explore technical methods in treating diversified effluents discharged from industrial units. Being toxic in nature, industrial wastewater effluents have several hazard effects on the ecosystems

Responsible Editor: Tito Roberto Cadaval Jr

✉ Sailesh N. Behera
sailesh.behera@snu.edu.in

¹ Environmental Engineering Laboratory, Department of Civil Engineering, Shiv Nadar University, Gautam Buddha Nagar, Delhi-NCR, Greater Noida, Uttar Pradesh 201314, India

² Centre for Environmental Sciences and Engineering (CESE), Shiv Nadar University, Greater Noida, Gautam Buddha Nagar, Uttar Pradesh 201314, India

of aquatic environment (Rathi et al. 2021). Among various industrial wastewater, the fate of wastewater released from textile industries is very complex due to its composition with more contents of organic dyes, which are typically self-resistant to degradation (Lellis et al. 2019; Kishor et al. 2021). This is noteworthy that most organic dyes are toxic and can cause cancer-like diseases and other harmful effects on humans, animals, and aquatic lives (Tkaczyk et al. 2020). Moreover, effluents generated from textile industries are responsible for deterioration of aquatic environment by polluting surface water and groundwater resources (Madhav et al. 2018; Kishor et al. 2021). In general, the effluent of the textile industry contains 30 to 50% unreacted dye molecules after use in production processes. This quantity of dye is adequate to obscure the sunlight onto the surface of water bodies, which would affect life cycle of the aquatic ecosystem (Arivoli et al. 2009).

The textile industrial sector is the highest consumer of raw water, and this demand has been increasing rapidly due to fast growth in production of textile products (Rather et al. 2019). As a result, the regular loadings of effluent discharge onto water bodies are also increasing proportionally. In the recent years of production process, it has been seen that processing 1 kg of fabric requires an average of 200–400 L of water and discharges significant amounts of wastewater (Amar et al. 2009). Depending on the application method, commercial dyes are classified into cationic, anionic, and nonionic types (Gadisa et al. 2019; Wang et al. 2022). Although it is difficult to provide precise information on types of dyes and annual production worldwide due to non-accessibility to specific data; currently, more than 100,000 types of commercial dyes exist and the production of 700,000–1,000,000 tons of commercial dyes are reported in literature (Mani et al. 2019). It has been observed that 90% of total dyes are used in textile industry, and remaining quantities are used in paper, plastic, leather, and chemical industries (Dawood and Sen 2014). The reported estimation shows that 280,000 tons of textile dyes (almost 30% of production) are finally discharged as industrial effluents annually (Ali 2010; Wang et al. 2022). Therefore, proper treatment of these discharged dyes through efficient and cost-effective techniques is necessary before they are discharged into the water bodies.

Many conventional techniques such as physical, chemical, and biological methods are usually practiced for treatment of textile industry effluents (Elgarahy et al. 2021; Shindhal et al. 2021). These methods include adsorption, adsorption on activated carbon materials, ion-exchange, irradiation, precipitation, ultra-filtration, membrane filtration, coagulation-flocculation, reverse osmosis, oxidation process, ozonation, Fenton's reagent, electrochemical destruction, and standard biological degradation processes (Kiran et al. 2019; Shindhal et al. 2021). These conventional methods

have several disadvantages for complete removal of dyes from effluents. Any biological treatment method needs a large area to accommodate different units with less flexibility in operations and design (Behera et al. 2021). Chemical treatment methods are costly due to requirement of expensive chemicals and electric power to maintain various units of operations (Shindhal et al. 2021). In those treatment methods, the sludge formed after the process has the potential to form secondary pollutants, which are more harmful than parent pollutants to humans, animals, and the aquatic environment (Saravanan et al. 2021). Therefore, adopting cost-effective process with less or no chemical requirement and negligible sludge formation after the process is essential for treating textile effluents.

In recent years, the adsorption process of dye removal is more acceptable because of its operational simplicity, economic effectiveness, higher efficiency, and accessibility to extensive adsorbents options (Behera et al. 2021; Mashabi et al. 2022). The technical understanding and application of nano-sized materials in eliminating dyes from textile effluents are increasing due to better significance (Mehta et al. 2021). Specifically, the adsorption process using magnetic nanoparticles as adsorbents has been assessed to be a capable treatment method due to its external magnet-assisted isolation of exhausted adsorbent material after treatment is done (Maaz et al. 2009; Elwakeel et al. 2016). CoFe_2O_4 and NiFe_2O_4 are the most useful magnetic materials due to facile synthesis steps; large mechanical hardness; lower toxicity; higher physical, chemical, and electrochemical stability; and moderate saturation magnetization that support a magnetic separation of adsorbent from treated effluents. Moreover, all these properties of CoFe_2O_4 and NiFe_2O_4 make them very robust adsorbents for textile effluent, while effluent possesses high alkaline or acidic nature.

The past reported studies (Selima et al. 2019; Mishra et al. 2020) used various methods including sol–gel, mechanical milling, combustion, hydrothermal, and ultrasonic-assisted hydrothermal process for synthesis of nanoparticles of CoFe_2O_4 and NiFe_2O_4 . However, co-precipitation method for preparation of these specific nanoparticles for further application in elimination of hazardous organic dyes such as TYG and AYR (used largely in India) is less reported or not completely understood in the literature. This is noteworthy that the co-precipitation method is more advantageous than other methods in providing highly crystalline, controlled shape, and small-sized particles (Selima et al. 2019; Kushwaha and Chauhan 2022). Although several studies (Santhosh et al. 2015; Shekari et al. 2017; Eskandarinezhad et al. 2021) were reported in application of CoFe_2O_4 and NiFe_2O_4 for removal heavy metals and other pollutants, elimination of organic dyes from both laboratory-prepared and real textile-industrial-effluent samples is lacking in the literature.

To fill the knowledge gaps in the literature for synthesis and characterization of nano-magnetic adsorbents for their further applications, this study is a first of its kind to examine the potential capabilities of CoFe_2O_4 and NiFe_2O_4 in elimination of hazardous organic dyes of TYG and AYR from both laboratory-prepared and real textile-industrial-effluent samples. The optimized conditions of the co-precipitation method (in accordance with temperature, pH, and initial adsorbent concentration) were adopted for synthesizing CoFe_2O_4 and NiFe_2O_4 . The characterization analysis of nanoparticles was performed using XRD, FTIR, FESEM-EDX, VSM, and BET techniques. CoFe_2O_4 and NiFe_2O_4 were employed as adsorbents for adsorption of TYG and AYR from laboratory-prepared and real textile-industrial-effluent samples. The adsorption mechanism was investigated through kinetics, equilibrium isotherms, and thermodynamics. The cost analysis for preparation of adsorbents and reusable capability of synthesized adsorbents was conducted.

Experimental details and methodology

Materials used, synthesis, and characterization of nanoparticles of CoFe_2O_4 and NiFe_2O_4

All chemicals required in conducting experimental runs in this study were of analytical grades, and we used those chemicals as delivered from the vendor without any further purification. The detailed chemical information of two selected organic dyes (TYG and AYR), mostly used in Indian textile industries, are provided in Table S1.

Nanoparticles of CoFe_2O_4 and NiFe_2O_4 were synthesized via co-precipitation method following procedures of previous studies (Maaz et al. 2009; Selima et al. 2019). In order to synthesis of NiFe_2O_4 , FeCl_3 and $\text{Ni}(\text{NO}_3)_2 \cdot 6\text{H}_2\text{O}$ were mixed in a 2:1 molar ratio with 100 ml of 0.2 M FeCl_3 and 100 ml of 0.1 M $\text{Ni}(\text{NO}_3)_2 \cdot 6\text{H}_2\text{O}$. Then, the mixed solution was kept at 60 °C followed by continuous constant stirring. A 3.0 M NaOH solution was added slowly in dropwise manner as a precipitating agent in the mixed solution resulting in maintaining a constant pH at 10. The resultant mixture was stirred constantly at 85 °C for 2 h until the desired solution was formed, followed by washing with acetone and oven drying at 120 °C for a duration of 10–16 h to get NiFe_2O_4 adsorbent. The oven dried NiFe_2O_4 nanoparticles were crushed and calcined at 500 °C for a duration of 5 h.

The XRD analysis of synthesized nanoparticles after annealing was investigated using BRUKER D8 Discover X-ray powder diffractometer. To determine saturation magnetization, coercivity, and remanent magnetization of nanoparticles, MicroSense EZ VSM instrumentation technique was used. Total surface area and pore volume

information of nanoparticles were quantified using Quanta chrome Autosorb 1C BET surface area and pore volume analyzer functioning at 77 K. The FESEM and EDX (Nova NanoSEM 450 FE-SEM) with magnification 50000X at 15 kV accelerating voltage was used to examine the surface morphology of nanoparticles. The spectral analysis of nanoparticles was conducted in the range from 4000 to 525 cm^{-1} through FT-IR instrument (Thermo-Electron Corporation, USA; A Nicolet iS20). Further descriptions are provided in the supplementary information.

Preparation of samples for treatment

The industrial samples were filtered multiple times to remove grit particles and maximum suspended solids. The desired quantities of TYG and AYR dyes were added to industrial wastewater samples. We used five different adsorbate dye samples, and their abbreviated names are described as follows: (i) TYG sample prepared from thiazole yellow G dye, (ii) AYR sample prepared from alizarin yellow R dye, (iii) mixture sample (MS) prepared with equal quantities of both thiazole yellow G and alizarin yellow dyes, (iv) industrial wastewater sample-A (IWWS-A) prepared from the effluent of industry outlet at site A, and (v) industrial wastewater sample-B (IWWS-B) prepared from the effluent of industry outlet at site B. Further descriptions are provided in the supplementary information.

Adsorption experiments for elimination of hazardous dyes

Every adsorption experiment was conducted in a 250 mL Erlenmeyer flask at a constant speed of 250 rpm and temperature of 25 °C through batch method using orbital shaker (Metrex MRS). About 3 mL of experimental solution was taken out at various time intervals, and adsorbent particles were separated using external magnet. All five adsorbate samples were studied to optimize the governing parameters of adsorption process including dosage of adsorbent, pH of solution, and contact time (Ahmed and Ahmaruzzaman, 2015). The initial pH values of the solution during adsorption were controlled through addition of desired quantity of 0.1 N or 0.1 N NaOH depending on targeted pH to be achieved. The exhausted adsorbent was isolated with an external magnet in the post-adsorption experiments. The left over dye concentration in the supernatant was calculated from observed values of absorbance measured at specified wavelengths using UV-Vis spectrophotometer for all related samples.

The removal or adsorption efficiency (%) of the adsorption process was estimated using Eq. (1), as

$$\text{Removal efficiency (\%)} = \frac{C_0 - C_t}{C_0} \times 100 \quad (1)$$

where C_0 represents initial concentration of dye (mg/L), and C_t represents concentration of dye at time (mg/L). We considered C_e as concentration of dye after equilibrium (mg/L) instead of C_t in an estimate of removal efficiency during adsorption process.

The quantity of adsorbed dye at any interval time of t (q_t) and after equilibrium achieved (q_e) in unit of mg/g was estimated using Eq. (2) and Eq. (3), as follows:

$$q_t = \frac{(C_0 - C_t) \times V}{m} \quad (2)$$

$$q_e = \frac{(C_0 - C_e) \times V}{m} \quad (3)$$

where V represents volume of solution in L, and m represents mass of adsorbent in g.

Results and discussion

Characterization of synthesized CoFe_2O_4 and NiFe_2O_4

XRD analysis

Figure 1(a) shows XRD patterns of synthesized nanoparticles. The diffraction patterns of CoFe_2O_4 and NiFe_2O_4 matched well with cubic spinel structure (JCPDS-ICDD 22–1086 and 010–0325) (Ristic et al. 2017; Chakradhary et al. 2019). As there were no other crystalline phases, single phase purity of these samples was indicated. The average crystallite sizes (D) of nanoparticles were determined from

Debye-Scherrer formula, as expressed in Eq. (4) using the most intense peak at 311 plane (Nabiyouni et al. 2010).

$$D = \frac{0.94\lambda}{\beta \cos \theta} \quad (4)$$

where D is crystallite size (nm), 0.94 is shape factor, λ is X-ray wavelength (nm), β is XRD line broadening at full width half (FWHM), and θ is Bragg's angle (radian).

CoFe_2O_4 showed the most intense peak at 311 plane at $2\theta = 35.60^\circ$, and other characteristic peaks appeared at $2\theta = 30.20^\circ, 43.31^\circ, 53.62^\circ, 57.26^\circ,$ and 62.89° , which could be indexed to the (h, k, l) planes of 220, 400, 422, 511, and 440, respectively. NiFe_2O_4 showed the most intense peak in 311 plane at $2\theta = 35.72^\circ$, and other characteristic peaks appeared at $2\theta = 30.33^\circ, 37.22^\circ, 43.40^\circ, 53.65^\circ, 57.39^\circ, 63.08^\circ,$ and 74.61° , which could be indexed to the (h, k, l) planes of 220, 222, 400, 422, 511, 440, and 533, respectively. The average crystallite size of CoFe_2O_4 and NiFe_2O_4 was calculated as 16.79 nm and 13.84 nm, respectively, from XRD analysis. The results observed in this study matched the range reported in the literature (Ristic et al. 2017; Chakradhary et al. 2019).

VSM analysis

As shown in Fig. 1(b), saturation magnetization, remanent magnetization, and coercivity for CoFe_2O_4 were obtained as 7.269 emu/g, 2.026 emu/g, and 142.43 Oe, respectively. Similarly, these parameters for NiFe_2O_4 were obtained as 6.61 emu/g, 0.294 emu/g, and 12.98 Oe, respectively. Thus, the measured magnetic parameters of nanoparticles exhibited ferromagnetic behavior at ambient temperature. The saturation magnetization of CoFe_2O_4 and NiFe_2O_4 was significantly lower because of fine particle sizes. The non-collinear spin arrangement in the particles was reflected in terms of

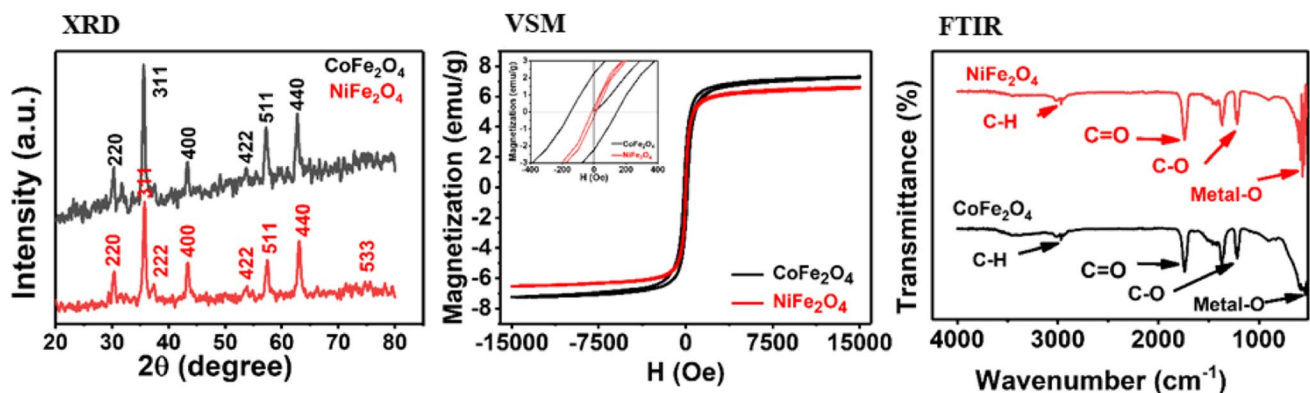


Fig. 1 XRD, VSM, and FTIR patterns of synthesized CoFe_2O_4 and NiFe_2O_4

low saturation magnetization. Similar trends of results of CoFe_2O_4 were reported in the literature (Margabandhu et al. 2017; Salavati-Niasari et al. 2009).

FTIR analytical results

Generally, FT-IR spectra are organized into two regions with characteristic region ($525\text{--}1000\text{ cm}^{-1}$) and functional group ($1000\text{--}4000\text{ cm}^{-1}$) region of relevant material. The bands that appeared below 1000 cm^{-1} represent the vibration of metal oxide bands (Pourgolmohammad et al. 2017). As depicted in Fig. 1(c), adsorbents were verified by the main absorption peaks observed in the range between 590 cm^{-1} and 569 cm^{-1} . The strong absorption band that appeared in the region $591\text{--}577\text{ cm}^{-1}$ corresponded to the stretching vibration of bonds between metal–oxygen at tetrahedral sites (Pourgolmohammad et al. 2017). The FT-IR bands that appeared below 1000 cm^{-1} are often validated to the stretching vibrations of metal ions in the crystal lattice structure (Ladgaonkar et al. 2002). The band near 1350 cm^{-1} appeared due to C–O stretching and observed

peak near 2900 cm^{-1} attributed to $-\text{CH}_2$ vibrations. CoFe_2O_4 and NiFe_2O_4 confirmed the preparation of spinel ferrite materials, which was also verified by XRD analysis.

FE-SEM analysis

From the observations of SEM images for CoFe_2O_4 (Fig. 2(a–b)), it was inferred that synthesized particles largely aggregated and possessed spherical shaped particles (Ristic et al. 2017). Figure 2(c–d) showed images of NiFe_2O_4 exhibited highly agglomerated with irregular shaped morphology (Saffari et al. 2015). The magnetic nature and their distribution influenced the particle size and shape of nanoparticles (Sharma et al. 2017). Figure S1(b–f; h–l) depicts images of elemental mappings of CoFe_2O_4 and NiFe_2O_4 , respectively. For CoFe_2O_4 , elements of cobalt, iron, and oxygen were homogeneously distributed in particles, which was evidenced from compiled image shown in Fig. S1(c). For NiFe_2O_4 , elements of nickel, iron, and oxygen were homogeneously distributed in particles, as shown in Fig. S1(i). Hence, it was inferred that homogeneous and uniform

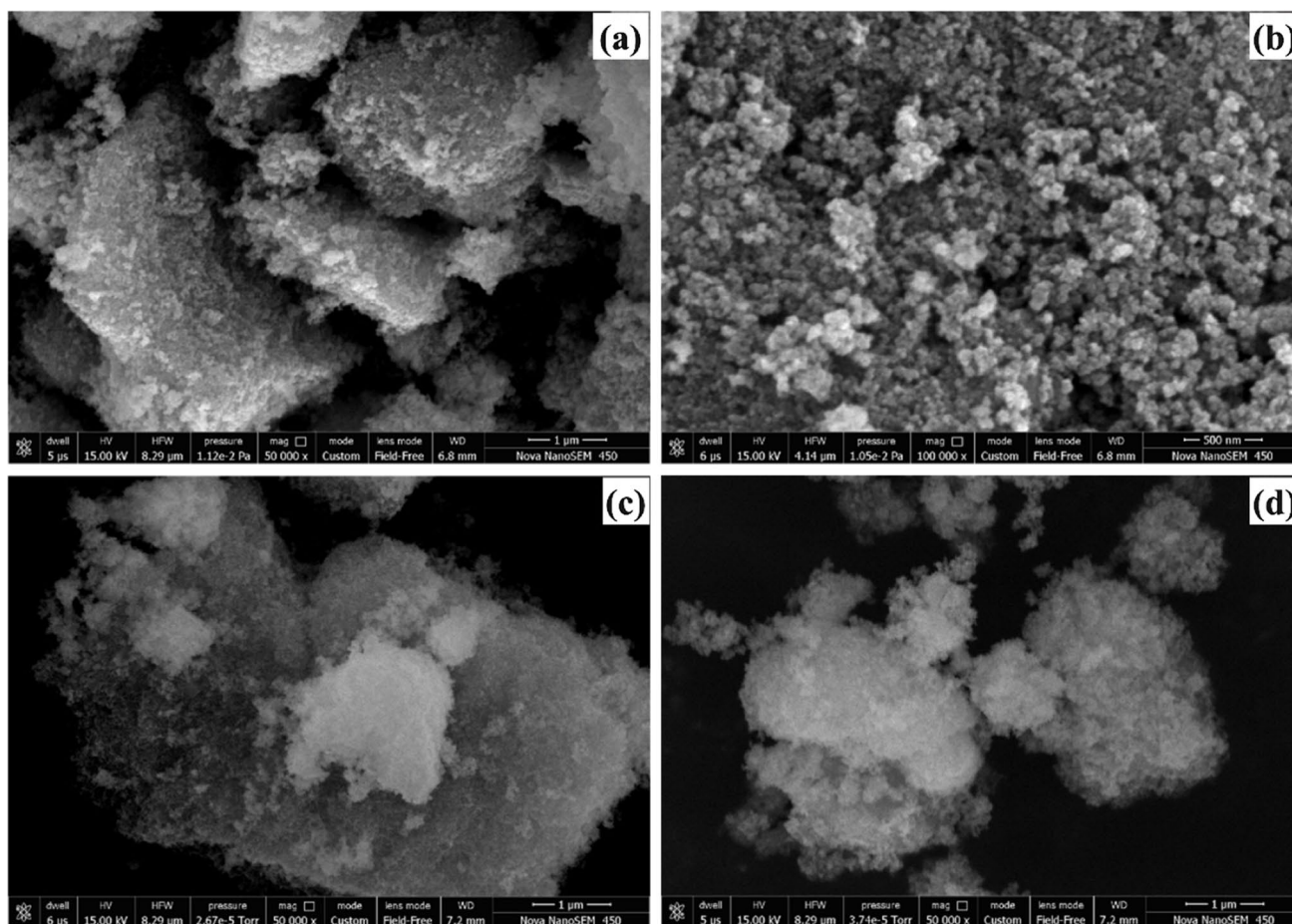


Fig. 2 FE-SEM images: (a, b) for CoFe_2O_4 samples and (c, d) for NiFe_2O_4 samples

distributions of elements were observed in the synthesized adsorbents (Das et al. 2018).

BET surface analysis

BET surface area of CoFe_2O_4 and NiFe_2O_4 was obtained as 64 and 62 m^2/g , respectively. Figure 3(a–b) depicts the hysteresis loop of N_2 adsorption–desorption isotherm plot of CoFe_2O_4 and NiFe_2O_4 , respectively. The nature of N_2 adsorption–desorption isotherm curve of CoFe_2O_4 and NiFe_2O_4 resembled with type IV isotherm (Zhu et al. 2016). The values of total pore volume and average pore radius of CoFe_2O_4 were 0.2935 cc/g and 92.24 Å , respectively. The values total pore volume and average pore diameter of NiFe_2O_4 are 0.3704 cc/g and 120.01 Å , respectively. The inner surface area of the adsorbents is mainly attributed to pore size distribution and pore volume, and it is a key feature affecting the adsorption efficiency (Ahmed et al., 2015). So, adsorbents with relatively smaller pore diameter than adsorbate molecule would restrict accumulation of adsorbate (Pelekani et al., 2000). The surface area of CoFe_2O_4 was previously reported by various researchers, such as 25 m^2/g at calcination of 550 $^\circ\text{C}$ by Silva et al. (2004), 22.15 m^2/g at

calcination of 500 $^\circ\text{C}$ by Sharma et al. (2019), and 13 m^2/g to 25 m^2/g at calcination 650 $^\circ\text{C}$ Paik et al. (2007). For NiFe_2O_4 , Li et al. (2014) reported the surface area of 20.1 m^2/g to 55.7 m^2/g , and Costa et al. (2006) reported 55.21 m^2/g surface area. We found relatively larger surface area of CoFe_2O_4 and NiFe_2O_4 , and hence, higher adsorption efficiency was expected for elimination of hazardous organic dye molecules. Further explanations are provided in the supplementary information.

Adsorption of dyes through treatment

Effect of pH on adsorption efficiency

Figure 4 shows the effect of solution pH on removal or adsorption efficiency of dyes for five different samples through adsorption using CoFe_2O_4 and NiFe_2O_4 . It was observed that the adsorption of dyes increased with decrease in pH of solution. The adsorption efficiency (%) of CoFe_2O_4 was obtained as 89, 86, 83, 79, and 76% for samples of TYG, AYR, MS, IWWS-A, and IWWS-B, respectively. Similarly, the adsorption efficiency (%) of NiFe_2O_4 was obtained as 90, 86, 82, 55, and 75%. Acidic (pH = 4) condition was

Fig. 3 Nitrogen adsorption desorption of: (a) CoFe_2O_4 and (b) NiFe_2O_4

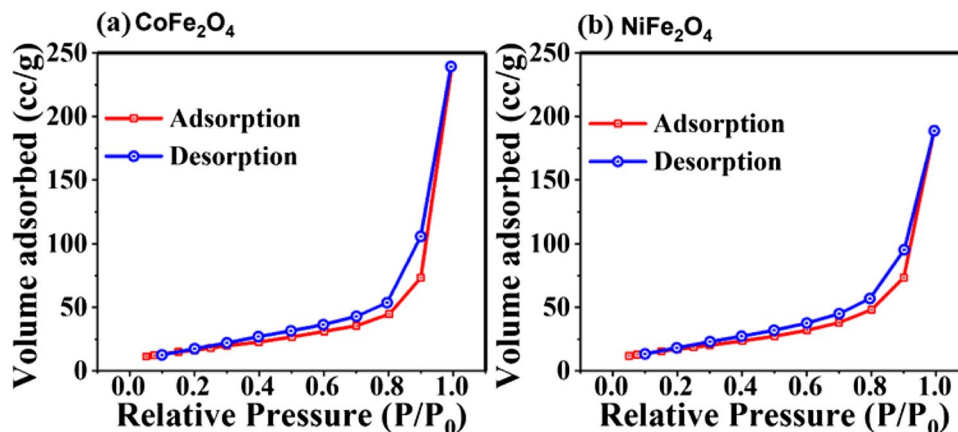
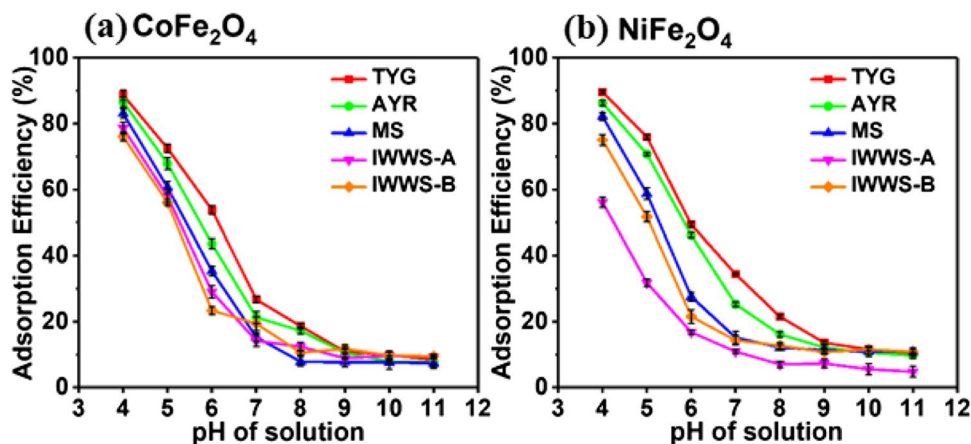


Fig. 4 Effect of pH of solution on adsorption efficiency: (a) CoFe_2O_4 and (b) NiFe_2O_4 . (Experimental conditions: adsorbent = 0.6 g/L , initial dye concentration = 30 mg/L , and time = 90 min)



significantly favorable for protonation on the surface of adsorbents. Due to protonation, positive charges on the surface of adsorbents were increased; hence, attraction forces between adsorbent surface and anionic pollutants significantly increased (Dogan and Mahir, 2003). The repulsion forces normally increase due to higher negative charge density in anionic pollutant solution at higher pH, and it is often unfavorable for adsorption of anionic dyes. Various adsorbent-adsorbate systems have been reported as a function of solution pH for adsorption process as an illustration (Rodríguez et al. 2009). Further explanations are provided in the supplementary information.

Effect of initial adsorbent concentration on adsorption efficiency

From the result shown in Fig. 5(a-b), it was observed that the maximum adsorption efficiency (%) of CoFe_2O_4 was found to be 98, 97, 93, 92, and 89% for TYG, AYR, MS, IWWS-A, and IWWS-B at optimum adsorbent dosage of 40, 40, 40, 40, and 50 mg, respectively. Similarly, the adsorption efficiency (%) of NiFe_2O_4 was found to be 96, 93, 92, 89, and 90 for TYG, AYR, MS, IWWS-A, and IWWS-B at a dosage of 40, 40, 70, and 40, respectively. The results expressed that

the adsorption efficiency increased with increase in amount of adsorbent due to availability of higher active sites for adsorption on the adsorbent surface (Wang et al. 2020). It is noteworthy that further adsorbent dosages did not provide any significant changes in removal of organic dyes from respective samples. Further explanations are provided in the supplementary information.

Effect of contact time on adsorption efficiency

Figure 6(a-b) shows the adsorption efficiency (%) plots of results with respect to time for all samples corresponding to adsorption by CoFe_2O_4 and NiFe_2O_4 , and insightful trends were observed for all samples with increasing first and then attaining steady state (Gupta et al. 2020). The experimental results revealed that the maximum adsorption efficiency of CoFe_2O_4 was attained as 98, 98, 92, 91, and 90% for dyes for samples of TYG, AYR, MS, IWWS-A, and IWWS-B, respectively. The maximum time for optimum adsorption due to CoFe_2O_4 was found to be 15, 15, 15, 30, and 35 min for samples of TYG, AYR, MS, IWWS-A, and IWWS-B, respectively. For NiFe_2O_4 , the maximum adsorption efficiency (%) of samples of TYG, AYR, MS, IWWS-A, and IWWS-B was achieved at as 95, 94, 92, 88,

Fig. 5 Effect of amount of adsorbent dosage on adsorption efficiency: (a) CoFe_2O_4 and (b) NiFe_2O_4 . (Experimental conditions: solution pH=4, initial dye concentration=30 mg/L, and time=90 min)

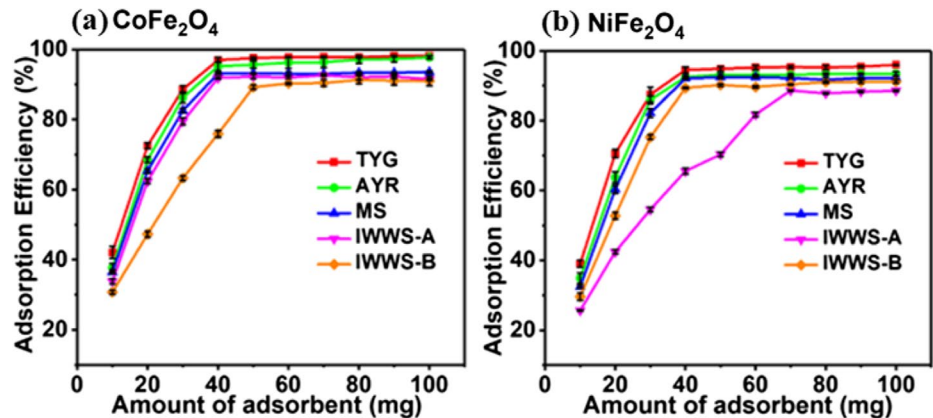
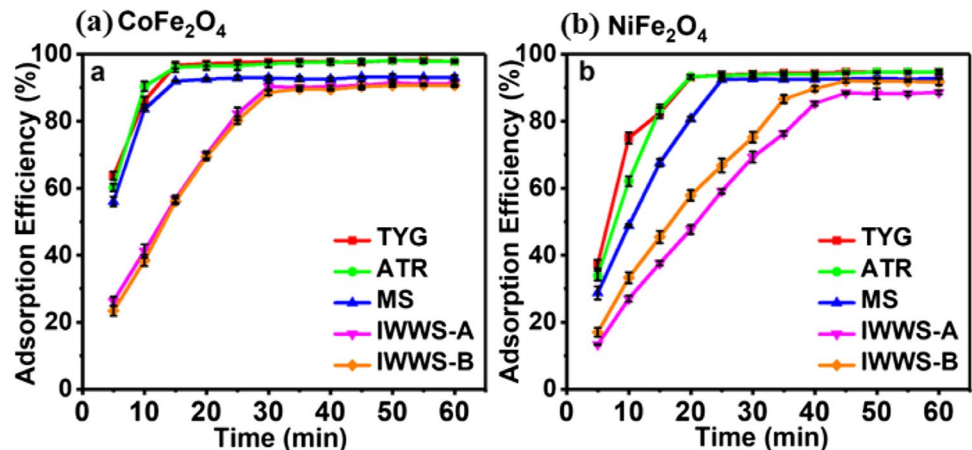


Fig. 6 Effect of contact time on adsorption efficiency: (a) CoFe_2O_4 ; and (b) NiFe_2O_4 . (Experimental conditions: solution pH=4, initial dye concentration=30 mg/L, and amount of adsorbent corresponding to adsorption systems were as follows: CoFe_2O_4 -TYG, CoFe_2O_4 -AYR, CoFe_2O_4 -MS, CoFe_2O_4 -IWWS-A, NiFe_2O_4 -TYG, NiFe_2O_4 -AYR, NiFe_2O_4 -MS, NiFe_2O_4 -IWWS-B at 0.8 g/L, CoFe_2O_4 -IWWS-B at 1.0 g/L, and NiFe_2O_4 -IWWS-A at 1.4 g/L)



and 90%, respectively, at time of 20, 20, 25, 45, and 40 min, respectively.

The removal of TYG, AYR, and their mixture from model samples was achieved significantly in a shorter time compared to industrial samples of IWWS-A and IWWS-B. The reason of such results could be due to various dissolved solids in industrial effluents. At initial stage, active sites might be available in large amount causing higher adsorption rate, and in progress of time, such binding site could be occupied resulting in slow down of adsorption rate (Mahapatra et al. 2013). Compared to model samples, IWWS-A and IWWS-B samples took more time to achieve maximum removal for both adsorbents. Individual removal of dyes of TYG and AYR was observed to be higher than the mixture sample of MS due to dye-dye interaction causing less removal efficiency in mixture sample. The removal of mixture dyes from laboratory samples was found to be higher than industrial samples of IWWS-A and IWWS-B containing mixture dyes. Overall observations from outcomes of this study implied that the adsorption of hazardous organic dyes depends on characteristics of wastewater samples and presence of active sites on the adsorbent surface. The presence of foreign entities and impurities in industrial samples could not interfere significantly in the adsorption process for elimination of hazardous organic dyes on the surface of adsorbents causing achievement of substantial removal of these dyes in industrial samples. It could be inferred that CoFe_2O_4 and NiFe_2O_4 removed hazardous organic dyes from industrial samples of IWWS-A and IWWS-B, indicating that the synthesized adsorbents in this study were quite effective in treatment of industrial effluents. More explanations and characteristics of industrial wastewater samples during treatment process are provided in the supplementary information.

Plausible adsorption mechanism of dye pollutants

The adsorbents of CoFe_2O_4 and NiFe_2O_4 are ferrite metal oxides, and the surface of these materials is normally shielded by $-\text{OH}$ group components that have the tendency to be fluctuated with their forms due to variations in pH values. As pH of dye-containing sample increases, the adsorption ratio decreases due to deprotonation of the adsorbent surfaces of the materials. Thus, subsequent deprotonation of $-\text{OH}$ group components occurs on the surface of adsorbent materials. This deprotonation leads to develop electrostatic repulsion between anionic dye molecule and adsorbent surface. In the range of alkaline nature of the solution pH, competition between $-\text{OH}$ group and dye anion occurs to occupy the active binding sites of adsorbent materials (Jethave et al. 2019; Afkhami and Moosavi 2010).

From this study, it could be suggested fundamentally that dye adsorption mechanism was based on electrostatic attraction between positive charge due to surface of adsorbent

material at an acidic medium and negative charge of dye molecule due to its anionic species characteristics. A graphical schematic representation of the adsorption mechanism of organic dyes of TYG and AYR onto surfaces of nanomaterial of CoFe_2O_4 and NiFe_2O_4 is depicted in Fig. 7. The aforementioned interpretation of results of variations of adsorption efficiency at various solution pH has been supported with such fundamental concepts of this mechanism of degradation of organic dyes resulting in proper treatment of laboratory and industrial samples. A significant electrostatic attraction exists between adsorbent and adsorbate at lower solution pH. The negative charge density on adsorbent increased with increase in pH of a solution, resulting in a significant decrease in adsorption efficiency through intensification of electrostatic repulsion between adsorbate and adsorbent at higher pH.

Adsorption equilibrium isotherms

We used experimental data in eight different adsorption isotherm models including Langmuir, Freundlich, Temkin, Elovich, Harkin-Jura, Redlich-Peterson, Dubinin-Raduskovich, and Jossens models to get insights into adsorption mechanism between adsorbents (CoFe_2O_4 and NiFe_2O_4) and adsorbate (TYG and AYR) systems.

The expressions of Langmuir isotherm model are provided in Eq. (5) (non-linear form) and Eq. (6) (linear form), as follows:

$$q_e = \frac{Q_0 b C_e}{1 + b C_e} \quad (5)$$

$$\frac{C_e}{q_e} = \frac{1}{Q_0 b} + \frac{C_e}{Q_0} \quad (6)$$

where, q_e represents adsorbate concentration on adsorbent after equilibrium (mg/g) (Eq. (3)). Q_0 represents the maximum amount of adsorption capacity of the adsorbent surface (mg/g), which correlates to complete monolayer accumulation. b represents Langmuir adsorption equilibrium constant (L/mg), related to free energy of adsorption. C_e represents adsorbate concentration in the solution at equilibrium (mg/L). The constants Q_0 and b were estimated from slopes and intercepts, respectively, of linear plots of C_e/q_e versus C_e (as demonstrated in Fig. 8).

An effective dimensionless parameter R_L (as expressed in Eq. (7)) represents essential characteristics of Langmuir model that helps in further assessment of adsorption process (Foo and Hameed 2010).

$$R_L = \frac{1}{1 + b C_0} \quad (7)$$

where C_0 represents initial adsorbate concentration (mg/L), and b is expressed earlier.

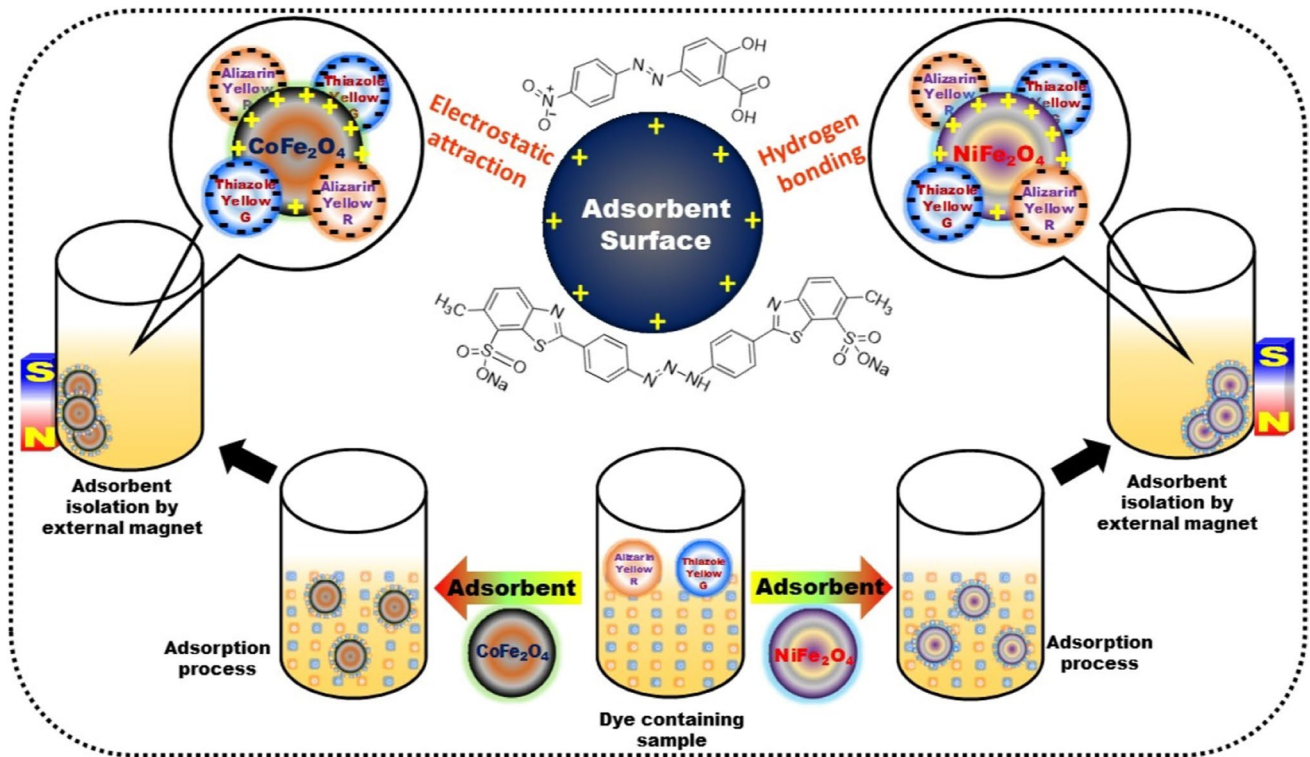
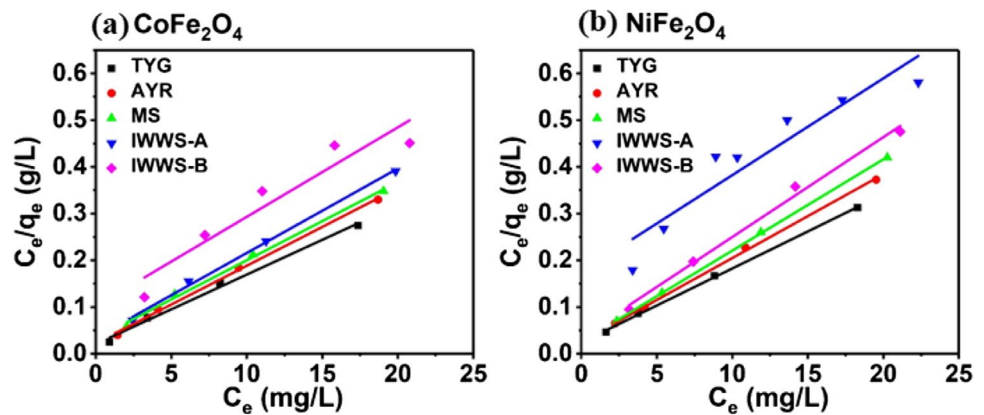


Fig. 7 Schematic of adsorption process and mechanism of TYG and AYR adsorption onto surfaces of CoFe_2O_4 and NiFe_2O_4

Fig. 8 Langmuir adsorption isotherm plots of TYG, AYR, MS, IWWS-A, and AWW-S-B samples of adsorbents of (a) CoFe_2O_4 and (b) NiFe_2O_4



The expressions of Freundlich isotherm model are provided in Eq. (8) (non-linear form) and Eq. (9) (linear form), as follows:

$$q_e = K_F C_e^{(1/n)} \tag{8}$$

$$\ln q_e = \ln K_F + \left(\frac{1}{n}\right) \ln C_e \tag{9}$$

where q_e is explained earlier. K_F represents Freundlich isotherm constant, related to adsorption capacity of adsorbent

in mg/g (Wang and Guo 2020). $1/n$ represents heterogeneity factor that is correlated to adsorption strength. C_e is explained earlier. To find out Freundlich constant, linear plots were made between $\ln q_e$ versus $\ln C_e$. The slope of plot was represented as n and intercept as $\ln K_f$ (depicted in Fig. S2(a) and Fig. S3(a)).

The linear expression of Temkin isotherm model is expressed in Eq. (10), as follows:

$$q_e = B_T \ln K_T + B_T \ln C_e \tag{10}$$

where, $B_T = \frac{RT}{b}$

where q_e is explained earlier. B_T is the constant related to heat of adsorption (J/mol). K_T is the binding constant at equilibrium, representing the maximum binding energy (L/g). T is absolute temperature (K), and R is the universal gas constant (8.314 J/mol.K). b is Temkin constant corresponding to adsorption energy (kJ/mol). C_e is explained earlier. To find out constants of Temkin model, linear plots were made between $\ln C_e$ versus q_e . Slope presents b and intercept was K_T in desired plot (depicted in Fig. S2(b) and Fig. S3(b)).

The linear form of Elovich model is expressed in Eq. (11) (Ayawei et al. 2017).

$$\ln \left(\frac{q_e}{C_e} \right) = \ln K_e q_m - \frac{q_e}{q_m} \quad (11)$$

where K_e represents Elovich constant, and q_m is Elovich's maximum adsorption ability, which can be determined from intercept and slope of the plot of $\ln(q_e/C_e)$ versus q_e (depicted in Fig. S2(c) and Fig. S3(c)).

The linear form of Redlich-Peterson isotherm model is expressed in Eq. (12).

$$\ln \left(\frac{C_e}{q_e} \right) = \beta \ln C_e - \ln A \quad (12)$$

where β and A represents the Redlich-Peterson exponent and constant. The plot of $\ln(C_e/q_e)$ versus $\ln C_e$ assists estimation of Redlich-Peterson constants, where β and A are obtained from slope and intercept, respectively, as depicted in Fig. S2(d) and Fig. S3(d) (Wu et al. 2010; Chan et al. 2012).

The expressions for Dubinin-Radushkevich isotherm model is provided in Eq. (13–14) (Vijayaraghavan et al. 2006).

$$\ln q_e = \ln q_s - K_{DR} \varepsilon^2 \quad (13)$$

$$\varepsilon = RT \ln \left(1 + \frac{1}{C_e} \right) \quad (14)$$

where ε is a Polanyi potential. R and T are explained earlier. β is Dubinin-Radushkevich constant and the parameters are determined as depicted in Fig. S2(e) and Fig. S3(e).

The reduced form of Jossens isotherm model represents Henry's law as expressed in Eq. (15) (Fritz and Schlueder 1974; Ayawei et al. 2017).

$$\ln \left(\frac{C_e}{q_e} \right) = -\ln H + F q_e^p \quad (15)$$

where H represents Jossens constant (corresponds to Henry's constant), F and p are Jossens isotherm constants, usually concerning irrespective of temperature and nature of adsorbents (depicted in Fig. S2(f) and Fig. S3(f)).

The expression of Harkin-Jura isotherm model is provided in Eq. (16) (Foo and Hameed 2010).

$$\frac{1}{q_e^2} = \frac{B}{A} - \frac{1}{A} \log C_e \quad (16)$$

where B and A are Harkin-Jura constants that can be estimated from plot of $1/q_e^2$ versus $\log C_e$ (depicted in Fig. S2(g) and Fig. S3(g)).

The assessment for applicability of isotherm adsorption models was performed through four evaluation parameters including residual sum of squares, Pearson's correlation coefficient, coefficient of determination (R^2), and R^2 Adj. Table S2 presents isothermal parameters and their results of evaluation assessment for adsorption of TYG, AYR, MS, IWWS-A, and IWWS-B samples onto surfaces of CoFe_2O_4 and NiFe_2O_4 . Figures 8, S2, and S3 show adsorption isotherms of TYG, AYR, MS, IWWS-A, and AWWS-B samples onto surfaces of CoFe_2O_4 and CoFe_2O_4 derived from Langmuir, Freundlich, Temkin, Elovich, Redlich-Peterson, Dubinin-Radushkevich, Jossens, and Harkin-Jura models. As Langmuir isotherm model fitted the best with all experimental results compared to other isotherm models, we plotted q_e versus C_e in non-linearized form for this model. Figures S4 and S5 show Langmuir non-linear adsorption isotherm of TYG, AYR, MS, IWWS-A, and AWWS-B samples onto surface of CoFe_2O_4 and NiFe_2O_4 , respectively. The results revealed that the values of maximum amount of adsorption capacity (Q_0 : mg/g) in linearized and non-linearized forms were not statistically different from each other at 95% level of confidence.

The comparison of coefficients of determination R^2 of linear form of Langmuir and Freundlich isotherm model indicated that Langmuir isotherm model gave better fit for all sets of experimental equilibrium adsorption results than Freundlich isotherm model. The maximum adsorption capacity of both adsorbent for all samples was estimated and presented in Table S2. The binding energies of all samples for adsorbents CoFe_2O_4 and NiFe_2O_4 are represented in Table S2. From the results of evaluated parameters (Table S2) for all isotherm models, it was observed that Langmuir adsorption isotherm model fitted well with better acceptance for adsorbent-adsorbate systems in this study. Compared to other isotherm models, Redlich-Peterson model gave more significant values of evaluating parameters than Langmuir, though this model is a hybrid version of Langmuir-Freundlich model. However, Elovich model did not show multi-layer adsorption; hence, Langmuir model was described well in this adsorption system for adsorption of organic dyes. The Langmuir dimensionless separation factor (R_L) indicates the nature of adsorption. The estimated R_L values indicated that the studied adsorbate-adsorbent systems were favorable in this study. More explanations about all adsorption isotherm models and model evaluating parameters are provided in the supplementary information.

Adsorption kinetics

We used pseudo-first-order, pseudo-second-order, intraparticle diffusion, and Elovich kinetic models to examine the uptake rate of organic dyes that normally influences residence time of sorption reaction and specific mechanism governed during adsorption of organic dyes onto the aqueous surfaces of CoFe_2O_4 and NiFe_2O_4 (Özacar et al. 2008; Rahdar et al. 2019; Patawat et al. 2020; Benjelloun et al. 2021). The experimental results were fit into all these four models to estimate kinetic parameters including rate constants of adsorption in the adsorbate-adsorbent systems.

The mathematical expressions of these four models are provided in Eqs. (17–20), as follows:

$$\ln(q_e - q_t) = \ln q_e - k_1 t \quad (17)$$

$$\frac{t}{q_t} = \frac{1}{k_2 q_e^2} + \frac{t}{q_e} \quad (18)$$

$$q_t = k_{id}(t)^{1/2} + C \quad (19)$$

$$q_t = \frac{1}{\beta} \ln(\alpha\beta) + \frac{1}{\beta} \ln(t) \quad (20)$$

The rate constants of pseudo-first-order, pseudo-second-order, intra-particle diffusion pseudo second-order, intraparticle diffusion, and Elovich kinetic models were represented as k_1 (min^{-1}), k_2 ($\text{g mg}^{-1} \text{min}^{-1}$), k_{id} ($\text{mg g}^{-1} \text{min}^{-1/2}$), and α ($\text{mg g}^{-1} \text{min}^{-1}$), respectively. q_t represents quantity of adsorbate adsorbed at time t (mg/g), and q_e represents quantity of adsorbate adsorbed at equilibrium (mg/g). C is intercept in plotting of intra-particle diffusion model. β represents chemisorption activation energy, which is related to surface coverage (g/mg).

The linear graph of $\ln(q_e - q_t)$ versus time (t) was plotted for all samples in Fig. 9(a-b) onto surfaces of CoFe_2O_4 and NiFe_2O_4 , respectively, for pseudo-first-order model. The values of k_1 and adsorption capacity were obtained from slope and intercept, respectively. The values of q_e and k_2 of pseudo-first-order model for all samples were determined from slopes and intercepts of plots of t/q_t versus t , respectively, as shown in Fig. 9(c-d). The coefficient of determination (R^2) used (to assess suitability of modeling and evaluate consistency between experimental and predicted data), k_1 and q_e (mg/g) of pseudo-first-order and pseudo-first-order models of all samples are presented in Table S3.

Figure 9(e-f) shows linear plots between q_e and $t^{(0.5)}$ for adsorption for all samples onto the surfaces of CoFe_2O_4 and NiFe_2O_4 , respectively, for intraparticle diffusion model. The results indicated that the straight line did not pass through the origin confirming that

intraparticle diffusion model is not the single rate controlling step. Thus, it represented the surface adsorption in the first stage with boundary layer diffusion and first trend-line with intraparticle diffusion in second layer trend-line (Özacar et al. 2008). The values of k_{id} , C , and R^2 for all samples of adsorption are provided in Table S3. Figure 9(g-h) shows linear plots between q_e and $\ln(t)$ for adsorption of all samples onto surfaces of CoFe_2O_4 and NiFe_2O_4 , respectively. For all organic dye samples, it was observed that pseudo-second-order kinetic model provided the best fit for experimental results with higher values of R^2 and predicted q_e values close to experimental values compared to other kinetic models (Table S3). Therefore, pseudo-second-order kinetics influenced the rate of uptake of organic dyes onto the surfaces of adsorbents to explain the mechanism of adsorption of TYG, AYR, MS, IWWS-A, and IWWS-B samples onto the surfaces of CoFe_2O_4 and NiFe_2O_4 in this study.

Thermodynamic study

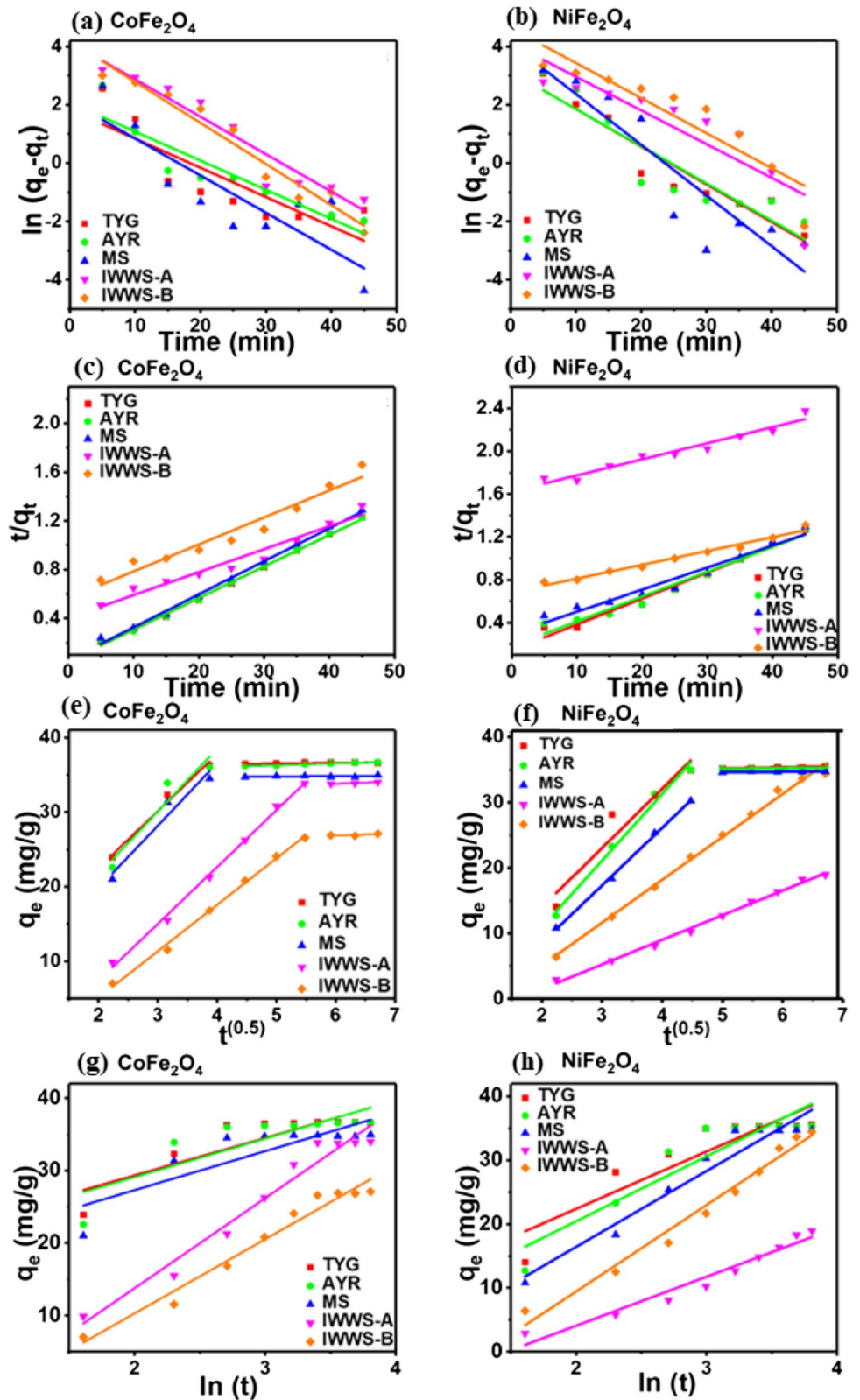
To examine the spontaneous nature and check the characteristics as exothermic or endothermic of required adsorption process on, we estimated thermodynamic parameters with variations in temperature (298, 303 and 308 K). Gibb's free energy change (ΔG°) was determined using mathematical expressions of Eqs. (21–22), as follows:

$$\Delta G = -RT \ln K_D \quad (21)$$

$$\ln K_D = \frac{\Delta S}{R} - \frac{\Delta H}{RT} \quad (22)$$

where T is solution temperature in kelvin, R is gas constant explained earlier. The thermodynamic equilibrium constant was evaluated from Langmuir isotherm based on procedures reported in literature (Lima et al. 2019). The $\ln K_D$ values were used to determine ΔG° at various temperature. The plot of $\ln K_D$ vs. $1/T$ was plotted using Van't Hoff equation. Its slope and intercept were used to determine thermodynamics parameters enthalpy (ΔH°) and entropy (ΔS°), respectively. The values of thermodynamic parameters for adsorption of TYG, AYR, MS, IWWS-A, and IWWS-B samples onto surfaces of CoFe_2O_4 and NiFe_2O_4 are presented in Table S4. The negative values of ΔH° and ΔG° indicated that adsorption process in the adsorbate-adsorbent system was exothermic and spontaneous in nature. The values of ΔG° for all adsorption systems increased with rise in temperature from 298 to 308 K, suggesting that adsorption process was not favorable at higher temperature. The negative entropy (ΔS°) indicated that adsorption process occurred systematically causing a decrease in randomness of adsorbate onto surface of adsorbent (Ghosal and Gupta et al., 2017).

Fig. 9 Adsorption kinetics of TYG, AYR, MS, IWWS-A, and IWWS-B samples onto surfaces of CoFe_2O_4 and NiFe_2O_4 : (a, b) pseudo-first-order model, (c, d) pseudo-second-order model, (e, f) intra-particle diffusion model, and (g, h) Elovich model



Regeneration and reuse of CoFe_2O_4 and NiFe_2O_4

In assessment of reusable capability of adsorbents of CoFe_2O_4 and NiFe_2O_4 , substantial number of regeneration experiments was conducted using alkaline solution with 1.0 M NaOH solution and calcination process at specific temperature, which was maintained during synthesis of these materials. Alkaline washing was further performed until supernatant became colorless at the end. Figure 10(a–b) depicts the results obtained from regeneration experiments for re-adsorption of organic dyes after four cycles of regeneration of CoFe_2O_4 and NiFe_2O_4 . A gradual reduction in re-adsorption efficiency (%) of organic dyes was observed after first and second runs. Nevertheless, re-adsorption efficiency percentage decreased significantly after third cycle of regeneration of adsorbents. The re-adsorption efficiency of adsorbent of CoFe_2O_4 was reduced from 97, 98, 93, 92, and 89% to 76, 74, 73, 69, and 64%, respectively, for TYR, AYR, MS, IWWS-A, and IWWS-B samples after fourth

cycle of regeneration. A similar trend in reduction in re-adsorption efficiency of adsorbent of NiFe_2O_4 was observed with reduction by 14, 13, 20, 20, and 17% for TYR, AYR, MS, IWWS-A, and IWWS-B samples, respectively, after fourth cycle of regeneration. The decreasing trend in re-adsorption efficiency of regenerated adsorbents could be attributed to significant loss in their adsorption capacities through reduction in crystallinity structure of materials. Moreover, repeated heating of materials can also be the reason for loss of crystallinity structure of materials causing inability to reconstruction of materials to their original stage (Ulbarri et al. 2001). From this experimental investigation, it was concluded that re-usable capability of both these adsorbent materials was prominent in elimination of hazardous organic dyes.

Cost analysis

In evaluation of the potential of synthesized nanomaterials as adsorbents for possible field application in treatment process after satisfying technical aspects, it is essential to assess cost analysis for fabrication of adsorbents. Based on the procedures reported in Das and Debnath (2022), we conducted cost analysis for synthesis of 1 kg of nanomaterials of CoFe_2O_4 and NiFe_2O_4 using cost of chemicals involved and energy required for heating and drying. We also considered other overhead cost as 10% of net cost and summed both these costs to arrive at total cost. Table S5 presents the details of breakup of cost involved for preparing 1 kg of adsorbents of CoFe_2O_4 and NiFe_2O_4 . The total cost for preparation of CoFe_2O_4 and NiFe_2O_4 was estimated to be \$ 267.42/kg and \$ 69.99/kg, respectively. Hence, the estimated cost for preparation of NiFe_2O_4 adsorbent was more affordable than CoFe_2O_4 adsorbent due to higher cost of involved chemicals. Comparing these results with the study of Das and Debnath (2022) in which fabrication cost of MgFe_2O_4 -PANI-NC was reported as \$142.52/kg for adsorption of methyl red dye, it could be inferred that lower cost of synthesis of CoFe_2O_4 and NiFe_2O_4 can be achieved with scale-up studies of these materials for future field application for treatment of industrial effluents discharged from textile industries.

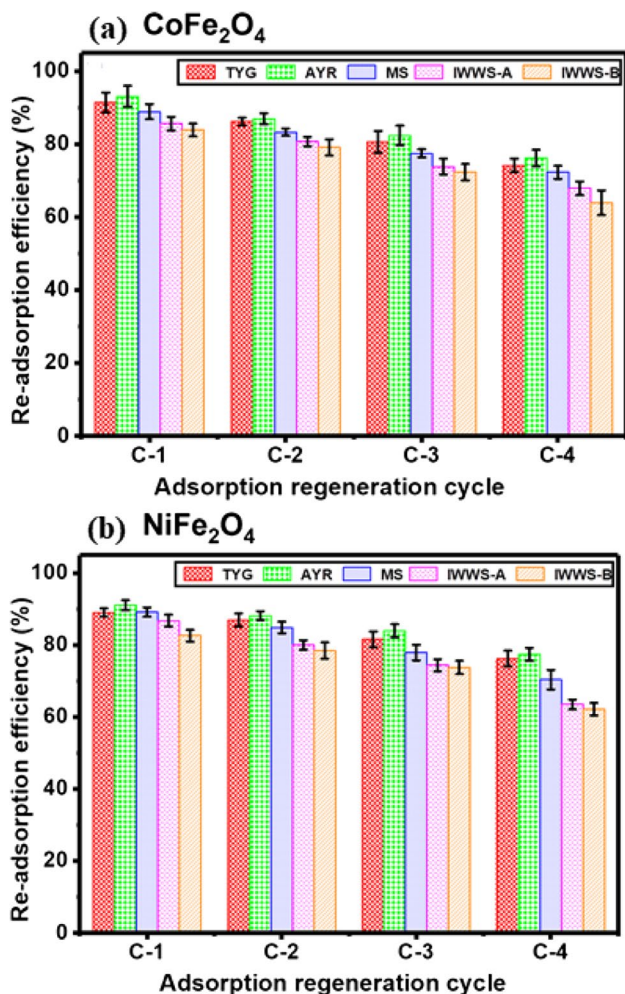


Fig. 10 Regeneration cycle with re-adsorption efficiency: (a) CoFe_2O_4 and (b) NiFe_2O_4

Conclusions

Magnetically separable nano-adsorbents of CoFe_2O_4 and NiFe_2O_4 were successfully synthesized by chemical co-precipitation technique, and these materials were employed in adsorption process to remove synthetic hazardous organic dyes of TYG and AYR from laboratory and industrial wastewater samples. Separate isolation technique was not required for adsorbent separation from the

solution after synthesis due to their magnetic property. Among all samples, optimum removal of single dye and binary mixture of dyes was obtained in an acidic medium. The amount of adsorbents and effective contact time for adsorption was investigated to arrive at optimum conditions for achieving the maximum adsorption efficiency in elimination of these hazardous pollutants. The results showed that CoFe_2O_4 and NiFe_2O_4 adsorbed organic dyes very rapidly during initial contact time followed by attaining the maximum efficiency and steady state trend. The adsorption isotherms modeling and kinetic study revealed that the adsorption process followed Langmuir adsorption isotherm and pseudo-second-order kinetics for all adsorbent-adsorbate systems. The re-usable capacity of both these materials was examined with satisfactory results up to fourth cycle of regeneration. The cost analysis of treatment process showed that such options can be a viable option to be studied with further scope of research for implementation as field applications. Thermodynamic analysis implied that the process involved in adsorbent-adsorbate systems for removal of organic dyes was exothermic and spontaneous in nature. The findings from this study suggested that nanoparticles of CoFe_2O_4 and NiFe_2O_4 can be used as effective adsorbents for efficient removal of hazardous organic dyes from the effluents of textile industries.

Supplementary Information The online version contains supplementary material available at <https://doi.org/10.1007/s11356-023-26059-5>.

Acknowledgements The authors gratefully acknowledge the support of Shiv Nadar University, Delhi-NCR in providing financial assistance in terms of Ph.D. scholarship to the first author and resources required for the operation of experiments and development of this manuscript. We are thankful to School of Natural Sciences, Shiv Nadar University for providing XRD and FTIR instrumentation facilities for analysis of materials. We gratefully acknowledge Advanced Center for Material Sciences at IIT Kanpur for providing BET analytical facility, and Scientium Analyze Solutions, Jaipur for providing VSM and FESEM instrumentations for analysis of materials.

Author contribution Dharmaraj J. Patil contributed to conceptualization, methodology development, conducting experiments, data analysis and processing, modeling work, and writing of the original manuscript. Sailesh N. Behera contributed to research guidance, frame-working scopes of research, conceptualization, resource generation, review, correction, and revision of the manuscript.

Data availability The relevant data are available from the authors through a reasonable approach.

Declarations

Ethics approval Not applicable.

Consent to participate Not applicable.

Consent for publication Not applicable.

Conflict of interest The authors declare no competing interests.

References

- Afkhami A, Moosavi R (2010) Adsorptive removal of Congo red, a carcinogenic textile dye, from aqueous solutions by maghemite nanoparticles. *J Hazard Mater* 174(1–3):398–403. <https://doi.org/10.1016/j.jhazmat.2009.09.066>
- Ahmed MJK, Ahmaruzzaman M (2015) A facile synthesis of Fe_3O_4 -charcoal composite for the sorption of a hazardous dye from aquatic environment. *J Environ Manage* 163:163–173. <https://doi.org/10.1016/j.jenvman.2015.08.011>
- Ajiboye TO, Oyewo OA, Onwudiwe DC (2021) Simultaneous removal of organics and heavy metals from industrial wastewater: a review. *Chemosphere* 262:128379. <https://doi.org/10.1016/j.chemosphere.2020.128379>
- Ali H (2010) Biodegradation of synthetic dyes—a review. *Water Air Soil Pollut* 213(1):251–273. <https://doi.org/10.1007/s11270-010-0382-4>
- Amar NB, Kechaou N, Palmeri J, Deratani A, Sghaier A (2009) Comparison of tertiary treatment by nanofiltration and reverse osmosis for water reuse in denim textile industry. *J Hazard Mater* 170(1):111–117. <https://doi.org/10.1016/j.jhazmat.2009.04.130>
- Arivoli S, Thenkuzhali M, Prasath P (2009) Adsorption of rhodamine B by acid activated carbon-kinetic, thermodynamic and equilibrium studies. *Orbital: Electron J Chem* 1(2):138–155
- Asgharnejad H, Khorshidi Nazloo E, Madani Larijani M, Hajinajaf N, Rashidi H (2021) Comprehensive review of water management and wastewater treatment in food processing industries in the framework of water-food-environment nexus. *Compr Rev Food Sci Food Saf* 20(5):4779–4815. <https://doi.org/10.1111/1541-4337.12782>
- Ayawei N, Ebelegi AN, Wankasi D (2017) Modelling and interpretation of adsorption isotherms. *J Chem*. <https://doi.org/10.1155/2017/3039817>
- Behera M, Nayak J, Banerjee S, Chakraborty S, Tripathy SK (2021) A review on the treatment of textile industry waste effluents towards the development of efficient mitigation strategy: an integrated system design approach. *J Environ Chem Eng* 9(4):105277. <https://doi.org/10.1016/j.jece.2021.105277>
- Benjelloun M, Miyah Y, Evrendilek GA, Zerrouq F, Lairini S (2021) Recent advances in adsorption kinetic models: their application to dye types. *Arab J Chem* 103031. <https://doi.org/10.1016/j.arabjc.2021.103031>
- Chakradhary VK, Ansari A, Akhtar MJ (2019) Design, synthesis, and testing of high coercivity cobalt doped nickel ferrite nanoparticles for magnetic applications. *J Magn Magn Mater* 469:674–680. <https://doi.org/10.1016/j.jmmm.2018.09.021>
- Chan LS, Cheung WH, Allen SJ, McKay G (2012) Error analysis of adsorption isotherm models for acid dyes onto bamboo derived activated carbon. *Chin J Chem Eng* 20(3):535–542. [https://doi.org/10.1016/S1004-9541\(11\)60216-4](https://doi.org/10.1016/S1004-9541(11)60216-4)
- Costa ACFM, Lula RT, Kiminami RHGA, Gama LFF, De Jesus AA, Andrade HMC (2006) Preparation of nanostructured NiFe_2O_4 catalysts by combustion reaction. *J Mater Sci* 41(15):4871–4875. <https://doi.org/10.1007/s10853-006-0048-1>
- Das I, Noori MT, Bhowmick GD, Ghangrekar MM (2018) Synthesis of bimetallic iron ferrite $\text{Co}_0.5\text{Zn}_0.5\text{Fe}_2\text{O}_4$ as a superior catalyst for oxygen reduction reaction to replace noble metal catalysts in microbial fuel cell. *Int J Hydrog Energy* 43(41):19196–19205. <https://doi.org/10.1016/j.ijhydene.2018.08.113>
- Das P, Debnath A (2022) Fabrication of MgFe_2O_4 /polyaniline nanocomposite for amputation of methyl red dye from water: Isotherm modeling, kinetic and cost analysis. *J Dispers Sci Technol*, 1–12. <https://doi.org/10.1080/01932691.2022.2110110>

- Dawood, S. and Sen, T. (2014). Review on dye removal from its aqueous solution into alternative cost effective and non-conventional adsorbents. *Journal of Chemical and Process Engineering*:1(104);1–11. <http://hdl.handle.net/20.500.11937/48131>
- Doğan M, Alkan M (2003) Adsorption kinetics of methyl violet onto perlite. *Chemosphere* 50(4):517–528. [https://doi.org/10.1016/S0045-6535\(02\)00629-X](https://doi.org/10.1016/S0045-6535(02)00629-X)
- Elgarahy AM, Elwakeel KZ, Mohammad SH, Elshoubaky GA (2021) A critical review of biosorption of dyes, heavy metals and metalloids from wastewater as an efficient and green process. *Clean Eng Technol* 4:100209. <https://doi.org/10.1016/j.clet.2021.100209>
- Elwakeel KZ, El-Bindary AA, El-Sonbati AZ, Hawas AR (2016) Adsorption of toxic acidic dye from aqueous solution onto diethylenetriamine functionalized magnetic glycidyl methacrylate-N, N'-methylenebisacrylamide. *RSC Adv* 6(4):3350–3361. <https://doi.org/10.1039/C5RA24035B>
- Eskandarinezhad S, Khosravi R, Amarzadeh M, Mondal P, Magalhães Filho FJC (2021) Application of different nanocatalysts in industrial effluent treatment: a review. *J Compos Compounds* 3(6):43–56
- Foo KY, Hameed BH (2010) Insights into the modeling of adsorption isotherm systems. *Chem Eng J* 156(1):2–10. <https://doi.org/10.1016/j.cej.2009.09.013>
- Fritz W, Schlueder EU (1974) Simultaneous adsorption equilibria of organic solutes in dilute aqueous solutions on activated carbon. *Chem Eng Sci* 29(5):1279–1282. [https://doi.org/10.1016/0009-2509\(74\)80128-4](https://doi.org/10.1016/0009-2509(74)80128-4)
- Gadisa BT, Appiah-Ntiamoah R, Kim H (2019) Amorphous iron sulfide nanowires as an efficient adsorbent for toxic dye effluents remediation. *Environ Sci Pollut Res* 26(3):2734–2746. <https://doi.org/10.1007/s11356-018-3811-3>
- Ghosal PS, Gupta AK (2017) Determination of thermodynamic parameters from Langmuir isotherm constant-revisited. *J Mol Liq* 225:137–146. <https://doi.org/10.1016/j.molliq.2016.11.058>
- Gupta A, Viltres H, Gupta NK (2020) Sono-adsorption of organic dyes onto CoFe₂O₄/graphene oxide nanocomposite. *Surf Interfaces* 20:100563. <https://doi.org/10.1016/j.surfin.2020.100563>
- Jethave G, Fegade U, Attarde S, Ingle S, Ghaedi M, Sabzehmeidani MM (2019) Exploration of the adsorption capability by doping Pb@ ZnFe₂O₄ nanocomposites (NCs) for decontamination of dye from textile wastewater. *Heliyon* 5(9):e02412. <https://doi.org/10.1016/j.heliyon.2019.e02412>
- Kamyab H, Yuzir MA, Abdullah N, Quan LM, Riyadi FA, Marzouki R (2022) Recent applications of the electrocoagulation process on agro-based industrial wastewater: a review. *Sustainability* 14(4):1985. <https://doi.org/10.3390/su14041985>
- Kiran S, Nosheen S, Abrar S, Anjum F, Gulzar T, Naz, S (2019) Advanced approaches for remediation of textile wastewater: a comparative study. *Advanced Functional Textiles and Polymers: Fabrication, Processing and Applications*, 201–264. <https://doi.org/10.1002/9781119605843.ch8>
- Kishor R, Purchase D, Saratale GD, Saratale RG, Ferreira LFR, Bilal M, Chandra R, Bharagava RN (2021) Ecotoxicological and health concerns of persistent coloring pollutants of textile industry wastewater and treatment approaches for environmental safety. *J Environ Chem Eng* 9(2):105012. <https://doi.org/10.1016/j.jece.2020.105012>
- Kushwaha P, Chauhan P (2022) Influence of different surfactants on morphological, structural, optical, and magnetic properties of α -Fe₂O₃ nanoparticles synthesized via co-precipitation method. *Appl Phys A* 128(1):1–14. <https://doi.org/10.1007/s00339-021-05157-6>
- Ladgaonkar BP, Kolekar CB, Vaingankar AS (2002) Infrared absorption spectroscopic study of Nd³⁺ substituted Zn-Mg ferrites. *Bull Mater Sci* 25(4):351–354. <https://doi.org/10.1007/BF02704131>
- Lellis B, Fávaro-Polonio CZ, Pamphile JA, Polonio JC (2019) Effects of textile dyes on health and the environment and bioremediation potential of living organisms. *Biotechnol Res Innov* 3(2):275–290. <https://doi.org/10.1016/j.biori.2019.09.001>
- Li DY, Sun YK, Gao PZ, Zhang XL, Ge HL (2014) Structural and magnetic properties of nickel ferrite nanoparticles synthesized via a template-assisted sol-gel method. *Ceram Int* 40(10):16529–16534
- Lima EC, Hosseini-Bandegharai A, Moreno-Piraján JC, Anastopoulos I (2019) A critical review of the estimation of the thermodynamic parameters on adsorption equilibria. Wrong use of equilibrium constant in the Van't Hoof equation for calculation of thermodynamic parameters of adsorption. *J Mol Liq* 273:425–434. <https://doi.org/10.1016/j.molliq.2018.10.048>
- Maaz K, Karim S, Mumtaz A, Hasanain SK, Liu J, Duan JL (2009) Synthesis and magnetic characterization of nickel ferrite nanoparticles prepared by co-precipitation route. *J Magn Magn Mater* 321(12):1838–1842. <https://doi.org/10.1016/j.jmmm.2008.11.098>
- Madhav S, Ahamad A, Singh P, Mishra PK (2018) A review of textile industry: wet processing, environmental impacts, and effluent treatment methods. *Environ Qual Manage* 27(3):31–41. <https://doi.org/10.1002/tqem.21538>
- Mahapatra A, Mishra BG, Hota G (2013) Adsorptive removal of Congo red dye from wastewater by mixed iron oxide–alumina nanocomposites. *Ceram Int* 39(5):5443–5451. <https://doi.org/10.1016/j.ceramint.2012.12.052>
- Mani S, Chowdhary P, Bharagava RN (2019) Textile wastewater dyes: toxicity profile and treatment approaches. In *Emerging and eco-friendly approaches for waste management*. Springer, Singapore, pp 219–244. https://doi.org/10.1007/978-981-10-8669-4_11
- Margabandhu, M., Sendhilnathan, S., Senthilkumar, S. and Gajalakshmi, D. (2017). Investigation of structural, morphological, magnetic properties and biomedical applications of Cu²⁺ substituted uncoated cobalt ferrite nanoparticles. *Braz Arch Biol Technol* 59. <https://doi.org/10.1590/1678-4324-2016161046>
- Mashabi RA, Khan ZA, Elwakeel KZ (2022) Chitosan or glycidyl methacrylate-based adsorbents for dyes removal from the aqueous solutions: a brief review. *Materials Advances*. <https://doi.org/10.1039/D2MA00320A>
- Mehta M, Sharma M, Pathania K, Jena PK, Bhushan I (2021) Degradation of synthetic dyes using nanoparticles: a mini-review. *Environ Sci Pollut Res* 28(36):49434–49446. <https://doi.org/10.1007/s11356-021-15470-5>
- Mishra S, Sahoo SS, Debnath AK, Muthe KP, Das N, Parhi P (2020) Cobalt ferrite nanoparticles prepared by microwave hydrothermal synthesis and adsorption efficiency for organic dyes: isotherms, thermodynamics and kinetic studies. *Adv Powder Technol* 31(11):4552–4562. <https://doi.org/10.1016/j.apt.2020.10.001>
- Nabiyouni G, Fesharaki MJ, Mozafari M, Amighian J (2010) Characterization and magnetic properties of nickel ferrite nanoparticles prepared by ball milling technique. *Chinese Physics Letters* 27(12):126401. <https://doi.org/10.1088/0256-307X/27/12/126401>
- Özacar M, Şengil İA, Türkmenler H (2008) Equilibrium and kinetic data, and adsorption mechanism for adsorption of lead onto valonia tannin resin. *Chem Eng J* 143(1–3):32–42. <https://doi.org/10.1016/j.cej.2007.12.005>
- Paik VV, Niphadkar PS, Bokade VV, Joshi PN (2007) Synthesis of spinel CoFe₂O₄ via the co-precipitation method using tetraalkyl ammonium hydroxides as precipitating agents. *J Am Ceram Soc* 90(9):3009–3012. <https://doi.org/10.1111/j.1551-2916.2007.01843.x>
- Patawat C, Silakate K, Chuan-Udom S, Supanchaiyamat N, Hunt AJ, Ngernyen Y (2020) Preparation of activated carbon from Dipterocarpus alatus fruit and its application for methylene blue adsorption. *RSC advances* 10(36):21082–21091. <https://doi.org/10.1039/D0RA03427D>

- Pelekani C, Snoeyink VL (2000) Competitive adsorption between atrazine and methylene blue on activated carbon: the importance of pore size distribution. *Carbon* 38(10):1423–1436. [https://doi.org/10.1016/S0008-6223\(99\)00261-4](https://doi.org/10.1016/S0008-6223(99)00261-4)
- Pourgolmohammad B, Masoudpanah SM, Aboutalebi MR (2017) Effects of the fuel type and fuel content on the specific surface area and magnetic properties of solution combusted CoFe_2O_4 nanoparticles. *Ceram Int* 43(11):8262–8268. <https://doi.org/10.1016/j.ceramint.2017.03.158>
- Rahdar S, Rahdar A, Zafar MN, Shafiqat SS, Ahmadi S (2019) Synthesis and characterization of MgO supported Fe–Co–Mn nanoparticles with exceptionally high adsorption capacity for Rhodamine B dye. *J Market Res* 8(5):3800–3810. <https://doi.org/10.1016/j.jmrt.2019.06.041>
- Rather LJ, Jameel S, Dar OA, Ganie SA, Bhat KA, Mohammad, F (2019) Advances in the sustainable technologies for water conservation in textile industries. In *Water in Textiles and Fashion* (pp. 175–194). Woodhead Publishing. <https://doi.org/10.1016/B978-0-08-102633-5.00010-5>
- Rathi BS, Kumar PS, Vo DVN (2021) Critical review on hazardous pollutants in water environment: occurrence, monitoring, fate, removal technologies and risk assessment. *Sci Total Environ* 797:149134. <https://doi.org/10.1016/j.scitotenv.2021.149134>
- Ristic M, Krehula S, Reissner M, Jean M, Hannoyer B, Musić S (2017) Synthesis and properties of precipitated cobalt ferrite nanoparticles. *J Mol Struct* 1140:32–38. <https://doi.org/10.1016/j.molstruc.2016.09.067>
- Rodríguez A, García J, Ovejero G, Mestanza M (2009) Adsorption of anionic and cationic dyes on activated carbon from aqueous solutions: equilibrium and kinetics. *J Hazard Mater* 172(2–3):1311–1320. <https://doi.org/10.1016/j.jhazmat.2009.07.138>
- Saffari F, Kameli P, Rahimi M, Ahmadvand H, Salamati H (2015) Effects of co-substitution on the structural and magnetic properties of $\text{NiCo}_x\text{Fe}_{2-x}\text{O}_4$ ferrite nanoparticles. *Ceram Int* 41(6):7352–7358. <https://doi.org/10.1016/j.ceramint.2015.02.038>
- Salavati-Niasari M, Davar F, Mahmoudi T (2009) A simple route to synthesize nanocrystalline nickel ferrite (NiFe_2O_4) in the presence of octanoic acid as a surfactant. *Polyhedron* 28(8):1455–1458. <https://doi.org/10.1016/j.poly.2009.03.020>
- Santhosh C, Kollu P, Felix S, Velmurugan V, Jeong SK, Grace AN (2015) CoFe_2O_4 and NiFe_2O_4 @ graphene adsorbents for heavy metal ions—kinetic and thermodynamic analysis. *RSC Adv* 5(37):28965–28972. <https://doi.org/10.1039/C5RA02905H>
- Saravanan A, Kumar PS, Jeevanantham S, Karishma S, Tajsabreen B, Yaashikaa PR, Reshma B (2021) Effective water/wastewater treatment methodologies for toxic pollutants removal: processes and applications towards sustainable development. *Chemosphere* 280:130595. <https://doi.org/10.1016/j.chemosphere.2021.130595>
- Selima SS, Khairy M, Bayoumy WA, Mousa MA (2019) Influence of preparation method on structural, optical, magnetic, and adsorption properties of nano- NiFe_2O_4 . *Environ Sci Pollut Res* 26(21):21484–21494. <https://doi.org/10.1007/s11356-019-05498-z>
- Sharma V, Chotia C, Ganesan V, Okram GS (2017) Influence of particle size and dielectric environment on the dispersion behaviour and surface plasmon in nickel nanoparticles. *Phys Chem Chem Phys* 19(21):14096–14106. <https://doi.org/10.1039/C7CP01769C>
- Sharma RP, Raut SD, Mulani RM, Kadam AS, Mane RS (2019) Sol-gel auto-combustion mediated cobalt ferrite nanoparticles: a potential material for antimicrobial applications. *Int Nano Lett* 9(2):141–147. <https://doi.org/10.1007/s40089-019-0268-4>
- Shekari H, Sayadi MH, Rezaei MR, Allahresani A (2017) Synthesis of nickel ferrite/titanium oxide magnetic nanocomposite and its use to remove hexavalent chromium from aqueous solutions. *Surfaces and Interfaces* 8:199–205. <https://doi.org/10.1016/j.surfin.2017.06.006>
- Shindhal T, Rakholiya P, Varjani S, Pandey A, Ngo HH, Guo W, Ng HY, Taherzadeh MJ (2021) A critical review on advances in the practices and perspectives for the treatment of dye industry wastewater. *Bioengineered* 12(1):70–87. <https://doi.org/10.1080/21655979.2020.1863034>
- Silva JB, De Brito W, Mohallem ND (2004) Influence of heat treatment on cobalt ferrite ceramic powders. *Mater Sci Eng, B* 112(2–3):182–187. <https://doi.org/10.1016/j.mseb.2004.05.029>
- Tkaczyk A, Mitrowska K, Posyniak A (2020) Synthetic organic dyes as contaminants of the aquatic environment and their implications for ecosystems: a review. *Science Total Environ* 717:137222. <https://doi.org/10.1016/j.scitotenv.2020.137222>
- Ulibarri MA, Pavlovic I, Barriga C, Hermosin MC, Cornejo J (2001) Adsorption of anionic species on hydroxalcalite-like compounds: effect of interlayer anion and crystallinity. *Appl Clay Sci* 18(1–2):17–27. [https://doi.org/10.1016/S0169-1317\(00\)00026-0](https://doi.org/10.1016/S0169-1317(00)00026-0)
- Vijayaraghavan K, Padmesh TVN, Palanivelu K, Velan M (2006) Biosorption of nickel (II) ions onto *Sargassum wightii*: application of two-parameter and three-parameter isotherm models. *J Hazard Mater* 133(1–3):304–308. <https://doi.org/10.1016/j.jhazmat.2005.10.016>
- Wang J, Guo X (2020) Adsorption kinetic models: physical meanings, applications, and solving methods. *J Hazard Mater* 390:122156. <https://doi.org/10.1016/j.jhazmat.2020.122156>
- Wang X, Jiang J, Gao W (2022) Reviewing textile wastewater produced by industries: characteristics, environmental impacts, and treatment strategies. *Water Sci Technol* 85(7):2076–2096. <https://doi.org/10.2166/wst.2022.088>
- Wu FC, Liu BL, Wu KT, Tseng RL (2010) A new linear form analysis of Redlich-Peterson isotherm equation for the adsorptions of dyes. *Chem Eng J* 162(1):21–27. <https://doi.org/10.1016/j.cej.2010.03.006>
- Zhu HY, Jiang R, Fu YQ, Li RR, Yao J, Jiang ST (2016) Novel multifunctional $\text{NiFe}_2\text{O}_4/\text{ZnO}$ hybrids for dye removal by adsorption, photocatalysis and magnetic separation. *Appl Surf Sci* 369:1–10. <https://doi.org/10.1016/j.apsusc.2016.02.025>

Publisher's note Springer Nature remains neutral with regard to jurisdictional claims in published maps and institutional affiliations.

Springer Nature or its licensor (e.g. a society or other partner) holds exclusive rights to this article under a publishing agreement with the author(s) or other rightsholder(s); author self-archiving of the accepted manuscript version of this article is solely governed by the terms of such publishing agreement and applicable law.